Applied Mathematical Modelling 109 (2022) 251–264

Contents lists available at ScienceDirect

Applied Mathematical Modelling

journal homepage: www.elsevier.com/locate/apm

Multi-field coupling solutions of functionally graded two-dimensional piezoelectric quasicrystal wedges and spaces

Xiang Mu[a,b], Wenshuai Xu[c,d], Zhaowei Zhu[a], Liangliang Zhang[a,*], Yang Gao[a,*]

[a] College of Science, China Agricultural University, Beijing 100083, China
[b] College of Engineering, China Agricultural University, Beijing 100083, China
[c] Key Laboratory of Microgravity, Institute of Mechanics, Chinese Academy of Sciences, Beijing 100190, China
[d] University of Chinese Academy of Sciences, Beijing 100049, China

ARTICLE INFO

Article history:
Received 15 August 2021
Revised 12 February 2022
Accepted 14 April 2022
Available online 18 April 2022

Keywords:
Infinite space
Functionally graded wedge
2D decagonal piezoelectric QCs
Wedge angle

ABSTRACT

Quasicrystal materials have aroused extensive attentions of researchers due to their excellent properties. In this paper, for the first time, functionally graded two-dimensional piezoelectric QC wedges and spaces which subjected to line force, charge or dislocation are investigated. By virtue of equilibrium and constitutive equations, the real form expressions of stresses and displacements are directly derived without introducing complex vectors. All expressions can be degraded to the classical solutions of homogeneous materials when material parameters have no concern with angle. Before the numerical results are presented, the comparative study between solutions of homogeneous materials from Stroh formalism and solutions of homogeneous materials from our method is performed to verify the accuracy of the formulation and numerical procedure. The mechanical behaviors of QC wedges and spaces under different loads are analyzed carefully by numerical examples. The numerical results reveal that the variations of stress and displacement in each field have much to do with the wedge angle and boundary conditions; line force has little effect on lattice rearrangement. Moreover, the numerical results can be used as references in engineering application when analyzing functionally graded materials.

1. Introduction

Quasicrystals (QCs) which have quasi-periodic long-range translational symmetry and long-range orientation symmetry were discovered by Levine and Shechtman in 1984 [1]. According to the arrangement of atoms, QCs can be defined as one-dimensional (1D), two-dimensional (2D) and three-dimensional (3D) QCs [2]. For example, the atom arrangement of 2D QCs possesses quasi-period in two directions and period in another direction. The unique atomic structures result in special physical and mechanical properties, such as high corrosion resistance [3], high wear resistance [4], high hardness [5] and low friction coefficient [6]. However, QCs also have the drawbacks of the high brittleness and low plasticity at room temperature [7], and these disadvantages prevent the QCs from being completely independent structural materials. Furthermore, QC materials have low thermal conductivity and negative temperature coefficients, and their thermal conductivity will be enhanced with higher temperature [8–11]. In practical applications, QCs can be used as composite reinforcement phases, non-stick coatings, thermal insulation materials, solar thin film materials, sensors and so on.

* Corresponding author.
E-mail addresses: llzhang@cau.edu.cn (L. Zhang), gaoyangg@gmail.com (Y. Gao).

https://doi.org/10.1016/j.apm.2022.04.018
0307-904X/

Piezoelectric effect is widely used in the field of electronic science and technology, such as sensors and actuators. Before the piezoelectric effect in QCs was discovered, many researchers [12–15] have done lots of studies for piezoelectric materials. Mohammad-Rezaei Bidgoli and Arefi [16] studied the problem of vibration for composite micro plate reinforced with functionally graded (FG) graphene nanoplatelets, by virtue of third-order shear deformation theory and modified strain-gradient theory, they obtained the maximum stiffness when graphene nanoplatelets are parabolic distribution and found that thermal loads have evident effect on natural frequencies. The Green's functions for transversely isotropic piezoelectric FG and multilayered half spaces are derived by Pan and Han [17] with the aid of propagator matrix method. Chen [18] explored the singularities of piezoelectric bonded wedge which subjected to thermal effect under mixed boundary using generalized Lekhnitskii formulation and Mellin transform. Arefi et al. [19] investigated 3D vibration analysis of a sandwich cylindrical shell containing an FG core and two FG piezoelectric layers by first-order shear deformation theory and Hamilton's principle. Zhou et al. [20] obtained the electro-elastic solutions of an elliptical hole in transversely isotropic piezoelectric material with complex potentials method, they found that sharp stress concentration existed near the hole. These theories and studies provide crucial theoretical reference and support for the researches of elastic, defects and multi-field coupling problems of QCs.

Considerable research efforts have been devoted to the theoretical analyzes of multi-field coupling problems of QCs since the discovery in 1984. Li et al. [21] investigated the QC material with eighteen-fold rotation symmetry properties, and constructed its constitutive and governing equations. They not only found that the phonon field is not coupled with the phason field, but also gave the expressions of the static elastic fields and dislocations. Wang and Pan [22] obtained a general solution for the dislocation problem of 1D hexagonal piezoelectric QCs. Li et al. [23] studied the basic solutions of the thermo-electro-elastic problem for 1D hexagonal QC, and got the 3D general solutions by using rigorous operator theory and Almansi's theorem. Meanwhile, they also obtained the Green's function solutions of this problem. Zhang et al. [24] studied thermoelastic plane problems of 2D decagonal QCs, and exhibited the formulas of phonon field, phason field and thermal field by virtue of Almansi's theorem. Li et al. [25] explored the FG multilayered 2D thermoelastic decagonal QC plates, especially analyzed the effects of the changes of FG exponential factor, coupling elastic constants and the thickness of QC layers on the phonon, phason and thermal fields of the plates. Yu et al. [26] investigated the plane piezoelasticity theory of 1D QCs which include all point groups by symmetry operations of point groups. Li et al. [27] proposed an analytical solution method to analyze arbitrarily shaped planar cracks which locates in 2D hexagonal QCs with thermal effects. Hu et al. [28] studied a partially-debonded circular inclusion in a 1D piezoelectric QC, and analyzed the influences of the crack angle and loads on the field singularities. These theoretical methods provide good inspiration for solving other planar problems, such as the multifield coupling problem of wedge shape.

Wedge is a piece of material with V-shaped edges. For the 2D plane problem, Xu and Rajapakse [29] studied the problems of piezoelectric wedges and multi-material wedges/junctions, and paid attention to examine the influence of wedge angle, polarization orientation, material types, and boundary and interface conditions on the order of singularity of electroelastic fields. Lv and Liu [30] considered the interaction between many parallel dislocations and a wedge-shaped crack in 1D hexagonal piezoelectric QC, they analyzed influence of wedge angle on the field intensity factors. Chen et al. [31] analyzed the singularity problem for piezoelectric-elastic wedges and junctions by specially developed 1D finite element formulation. Hwu and Ikeda [32] explored the cracks of piezoelectric materials by solutions of piezoelectric multi-wedges. In addition, they also extended the stress/electric intensity factors which were defined for cracks, interface cracks and interface corners to normal angles. Hwu [33] and Ting [34] have discussed the solutions for the wedge of general anisotropic material at critical wedge angles.

Stroh formalism [34–37] is a powerful approach to deal with 2D deformation problems. However, the Stroh formalism does not apply to inhomogeneous materials [38–40], such as FG materials. Here, a different approach [39,40], the surface traction on any radial plane is invariant with θ, is employed and the general anisotropic problem is extended to more complex QC problem. The analytical expressions of displacements and stresses are derived by considering stresses are proportional to r^{-1}, and the effects of different loads on stresses, displacements and electric field are analyzed in detail. What's more, the FG 2D piezoelectric QC can be degraded to homogeneous piezoelectric QC, which is compared with literature results to verify the correctness of method and numerical results. The approach employed here can be used to solve singularity problems, such as angularly inhomogeneous piezoelectric composite wedges, an infinite plane containing two different half-planes and the composite wedges including several inhomogeneous anisotropic wedges.

2. Basic equations and the key equations

According to the elastic theory of QCs [41–43], the basic equations without body force of 2D piezoelectric QCs are expressible as

$$\varepsilon_{kl} = \frac{1}{2}\left(\frac{\partial u_k}{\partial x_l} + \frac{\partial u_l}{\partial x_k}\right),\ w_{\alpha l} = \partial_l w_\alpha, E_l = -\partial_l \phi, \tag{1}$$

$$\begin{aligned} \sigma_{ij} &= C_{ijkl}\varepsilon_{kl} + R_{ij\alpha l}w_{\alpha l} - e_{lij}E_l, \\ H_{\beta j} &= R_{kl\beta j}\varepsilon_{kl} + K_{\beta j\alpha l}w_{\alpha l}, \\ D_j &= e_{jkl}\varepsilon_{kl} + \chi_{jl}E_l, \end{aligned} \tag{2}$$

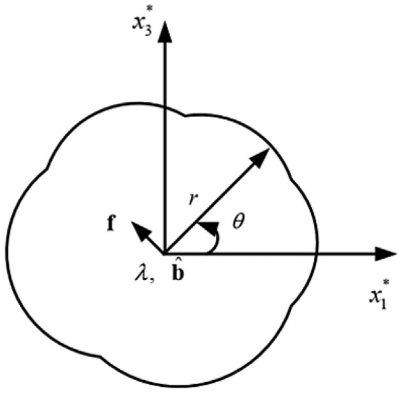

Fig. 1. The infinite FG space subjected to line force $\mathbf{f}$, charge λ and Burgers vector $\hat{\mathbf{b}}$ at the origin $r = 0$.

$$\partial_j \sigma_{ij} = 0,\ \partial_j H_{\beta j} = 0,\ \partial_j D_j = 0, \tag{3}$$

where $i, j, k, l = 1, 2, 3$, $\alpha, \beta = 1, 2$. The phonon displacementsu_k denote atomic translation, but the phason displacements w_α denote rearrangements of atoms along the quasi-period directions [43]. Furthermore, σ_{ij}, $H_{\beta j}$, D_j and ϕ are the phonon stresses, phason stresses, electric displacements and electric potential, respectively; ε_{kl}, $w_{\alpha l}$, E_l represent the phonon strains, phason strains and electric field intensities, respectively; C_{ijkl}, $K_{\beta j\alpha l}$ are the elastic constants in phonon and phason fields, respectively; $R_{ij\alpha l}$ are the coupling elastic constants; e_{lij} are the piezoelectric constants in the phonon field; χ_{jl} are the dielectric constants.

In polar coordinates

$$x_1 = r\cos\theta,\ x_3 = r\sin\theta,\ x_2 = z. \tag{4}$$

It is assumed that the material constants of the FG 2D piezoelectric QC follow the exponential function law [44] with respect to θ. Then,

$$C_{ijkl} = C^0_{ijkl}e^{\eta\theta},\ K_{\beta j\alpha l} = K^0_{\beta j\alpha l}e^{\eta\theta},\ R_{ij\alpha l} = R^0_{ij\alpha l}e^{\eta\theta},\ e_{lij} = e^0_{lij}e^{\eta\theta},\ \chi_{jl} = \chi^0_{jl}e^{\eta\theta}, \tag{5}$$

where η is an FG exponential factor. The superscript "0" represents the initial material constants which are independent of θ. We have the following properties that

$$\begin{aligned} &C_{ijkl} = C_{jikl} = C_{klij} = C_{ijlk},\ K_{\beta j\alpha l} = K_{\alpha l\beta j},\ R_{ij\alpha l} = R_{ji\alpha l},\ e_{lij} = e_{lji},\ \chi_{jl} = \chi_{lj},\ C_{ijkl}\varepsilon_{ij}\varepsilon_{kl} > 0,\\ &\quad K_{\beta j\alpha l}w_{\beta j}w_{\alpha l} > 0,\ \chi_{jl}E_jE_l > 0. \end{aligned} \tag{6}$$

In present work, we consider the generalized 2D problem which means that all field variables are dependent on x_1 and x_3. Two typical problems are considered, problem A: an infinite FG 2D piezoelectric QC space is subjected to line force, charge and line dislocation at the origin$r = 0$; problem B: an FG 2D piezoelectric QC wedge of wedge angle $\alpha(0 \le \theta \le \alpha)$, which two sides are traction free, subjected to the line force and charge at the wedge apex $r = 0$.

In order to simplify the calculation process, the generalized displacement vector is introduced

$$\mathbf{u} = [u_1, u_2, u_3, w_1, w_2, \phi]^T, \tag{7}$$

where the superscript "T" denotes the transpose of the matrix. Hence, the constitutive equations and the equilibrium equations are expressed as

$$\sigma_{Ij} = E_{IjKl}u_{K,l}, \sigma_{Ij,j} = 0 (I, K = 1, 2, 3, 4, 5, 6;\ j, l = 1, 2, 3), \tag{8}$$

$$\begin{aligned} u_K &= u_K (K = 1, 2, 3),\ u_K = w_{K-3} (K = 4, 5),\ u_K = \phi (K = 6),\\ \sigma_{Ij} &= \sigma_{Ij} (I = 1, 2, 3),\ \sigma_{Ij} = H_{(I-3)j} (I = 4, 5),\ \sigma_{Ij} = D_j (I = 6),\\ E_{IjKl} &= C_{IjKl} (I, K = 1, 2, 3),\ E_{IjKl} = K_{(I-3)j(K-3)l} (I, K = 4, 5),\\ E_{IjKl} &= R_{Ij(K-3)l} (I = 1, 2, 3; K = 4, 5),\ E_{IjKl} = R_{(I-3)jKl} (I = 4, 5; K = 1, 2, 3),\\ E_{IjKl} &= e_{Ijl} (I = 1, 2, 3; K = 6),\ E_{IjKl} = e_{jKl} (I = 6; K = 1, 2, 3),\\ E_{IjKl} &= -\chi_{jl} (I, K = 6). \end{aligned} \tag{9}$$

Figures 1 and 2 describe the situations of problem A and problem B, respectively. The line force $\mathbf{f}$ and free charge density λ act at $r = 0$; $\hat{\mathbf{b}}$ denotes Burgers vector.

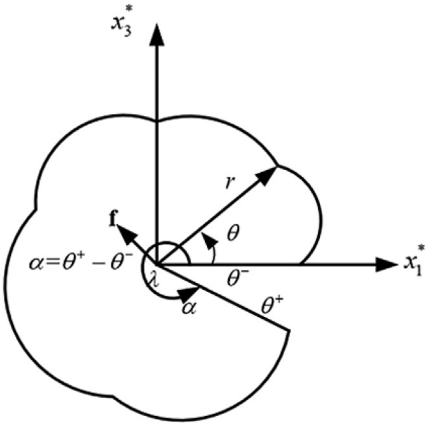

Fig. 2. The FG piezoelectric QC wedge with wedge angle α, subjected to line force and charge at the wedge apex $r = 0$.

According to the literature [45] and Eq. (A1), the stresses are proportional to r^{-1}, so we get

$$\sigma_{\alpha j} = \frac{1}{r}\xi_{\alpha j}(\theta), (\alpha = 1, 2, 3, 4), \tag{10}$$

$$H_{\gamma j} = \frac{1}{r}\varsigma_{\gamma j}(\theta), (\gamma = 1, 2, j = 1, 2, 3), \tag{11}$$

where $\sigma_{\alpha j}$ denote stresses in the phonon field and electric displacement, $H_{\gamma j}$ denote stresses in the phason field, $\xi_{\alpha j}$ and $\varsigma_{\gamma j}$ vary with the angle θ.

Substituting Eqs. (10) and (11) into the equilibrium Eq. (3), we get

$$\frac{1}{r}\left[-\frac{1}{r}\frac{\partial r}{\partial x_j}\xi_{\alpha j}(\theta) + \xi_{\alpha j}(\theta)_{,\theta}\frac{\partial \theta}{\partial x_j}\right] = 0, \tag{12}$$

$$\frac{1}{r}\left[-\frac{1}{r}\frac{\partial r}{\partial x_j}\varsigma_{\gamma j}(\theta) + \varsigma_{\gamma j}(\theta)_{,\theta}\frac{\partial \theta}{\partial x_j}\right] = 0. \tag{13}$$

With the aid of Eqs. (A2), (12) and (13) can be rewritten as

$$\frac{1}{r^2}\left[\left(\xi_{\alpha j}(\theta)m_j\right)_{,\theta}\right] = 0, \tag{14}$$

$$\frac{1}{r^2}\left[\left(\varsigma_{\gamma j}(\theta)\right)m_j\right)_{,\theta}\Big] = 0. \tag{15}$$

By Eqs. (14) and (15), we get

$$\zeta_{Ij}(\theta)m_j = \frac{1}{\pi}p_I(I = 1, 2, 3, 4, 5, 6), \tag{16}$$

where $\zeta_{Ij}(\theta)(I = 4, 5)$ and $\zeta_{Ij}(\theta)(I = 6)$ in connection with the phason field and electric field, respectively, p_I is a constant column vector.

Assuming that $\mathbf{t}_\theta$ is the surface traction vector on the radial plane θ = constant, through $(\mathbf{t}_\theta)_\alpha = \sigma_{\alpha j}m_j$, $(\mathbf{t}_\theta)_\gamma = H_{\gamma j}m_j$ and Eqs. (10), (11), we obtain

$$(\mathbf{t}_\theta)_I = \frac{1}{r}\zeta_{Ij}(\theta)m_j = \frac{1}{\pi r}p_I. \tag{17}$$

Eq. (17) can be expressed as

$$\mathbf{t}_\theta^T = \frac{1}{\pi r}\mathbf{p}^T. \tag{18}$$

Take the form of displacement $\mathbf{u}$

$$\mathbf{u} = -\frac{1}{\pi}(\ln r)\mathbf{q} + \boldsymbol{\nu}(\theta), \tag{19}$$

where $\mathbf{q}$ is a constant column vector and $\boldsymbol{\nu}(\theta)$ depends on θ. Considering the component form of Eq. (19), we have

$$u_k = -\frac{\ln r}{\pi}q_k + \nu_k(\theta)(k = 1, 2, 3, 4, 5, 6), \tag{20}$$

where $k = 4, 5, 6$ denote displacements in the phason field and electric potential, respectively. Substituting Eq. (20) into Eq. (2), and using Eqs. (A2), (5), (9) (10), (11) and (17) we get

$$e^{\eta\theta}\left(-\frac{1}{\pi}E^0_{IjKl}m_jn_lq_k + E^0_{IjKl}m_jm_l\frac{\partial v_k(\theta)}{\partial\theta}\right) = \frac{1}{\pi}p_I, \tag{21}$$

Eq. (21) can be expressed in matrix form

$$-\frac{1}{\pi}\mathbf{R}^T(\theta)\mathbf{q} + \mathbf{T}(\theta)\boldsymbol{v}(\theta)_{,\theta} = \frac{1}{\pi}\mathbf{p}. \tag{22}$$

Let

$$\left.\begin{aligned} Q_{IK}(\theta) &= e^{\eta\theta}E^0_{IjKl}n_jn_l \\ R_{IK}(\theta) &= e^{\eta\theta}E^0_{IjKl}n_jm_l \\ T_{IK}(\theta) &= e^{\eta\theta}E^0_{IjKl}m_jm_l \end{aligned}\right\}, \tag{23}$$

$$R^T_{IK}(\theta) = R_{KI}(\theta) = e^{\eta\theta}E^0_{IjKl}m_jn_l. \tag{24}$$

It should be pointed out that $\mathbf{Q}(\theta)$ and $\mathbf{T}(\theta)$ are symmetric. Introducing the 6×6 matrices

$$\left.\begin{aligned} \mathbf{N}_1(\theta) &= -\mathbf{T}^{-1}(\theta)\mathbf{R}^T(\theta) \\ \mathbf{N}_2(\theta) &= \mathbf{T}^{-1}(\theta) \\ \mathbf{N}_3(\theta) &= \mathbf{R}(\theta)\mathbf{T}^{-1}(\theta)\mathbf{R}^T(\theta) - \mathbf{Q}(\theta) \end{aligned}\right\}, \tag{25}$$

where $\mathbf{N}_2(\theta)$ and $\mathbf{N}_3(\theta)$ are symmetric, Eq. (22) can be simplified as

$$\boldsymbol{v}(\theta)_{,\theta} = \frac{1}{\pi}[\mathbf{N}_2(\theta)\mathbf{p} - \mathbf{N}_1(\theta)\mathbf{q}]. \tag{26}$$

Eq. (26) is integrated from 0 to θ, and using Eq. (A4) to yield,

$$\boldsymbol{v}(\theta) = \mathbf{H}(\theta)\mathbf{p} - \mathbf{S}(\theta)\mathbf{q}. \tag{27}$$

With the aid of Eqs. (19) and (27), we obtain

$$\mathbf{u} = -\frac{\ln r}{\pi}\mathbf{q} - \boldsymbol{S}(\theta)\mathbf{q} + \mathbf{H}(\theta)\mathbf{p}, \tag{28}$$

where $\mathbf{p}$ and $\mathbf{q}$ are unknown arbitrary vectors, but they can be determined by boundary conditions.

Through $(\mathbf{t}_r)_\alpha = \sigma_{\alpha j}n_j$,$(\mathbf{t}_r)_\gamma = H_{\gamma j}n_j$, surface traction $\mathbf{t}_r$ on the surface $r =$ constant is denoted as

$$(\mathbf{t}_r)_I = \frac{1}{r}e^{\eta\theta}\left(-\frac{1}{\pi}E^0_{IjKl}n_jn_lq_k + E^0_{IjKl}n_jm_l\frac{\partial v_k(\theta)}{\partial\theta}\right). \tag{29}$$

Eqs. (23), (25), (26) and (29) are used to obtain

$$\mathbf{t}_r = \frac{1}{\pi r}\left[\mathbf{N}_3(\theta)\mathbf{q} - \mathbf{N}_1^T(\theta)\mathbf{p}\right]. \tag{30}$$

According to the equilibrium Eq. (3), we get

$$\begin{aligned} &\sigma_{\alpha 1} = -\varphi_{\alpha,3}, \sigma_{\alpha 3} = \varphi_{\alpha,1}, \\ &H_{\gamma 1} = -\varphi_{\gamma,3}, H_{\gamma 3} = \varphi_{\gamma,1}, \end{aligned} \tag{31}$$

where $\boldsymbol{\varphi}$ is the stress function.

In polar coordinates, we have

$$(\mathbf{t}_r)_I = -\frac{\partial}{r\partial\theta}\varphi_I, (\mathbf{t}_\theta)_I = \frac{\partial}{\partial r}\varphi_I. \tag{32}$$

Therefore, the generalized traction vectors can be denoted as

$$\mathbf{t}_r = -\frac{\partial}{r\partial\theta}\boldsymbol{\varphi}, \mathbf{t}_\theta = \frac{\partial}{\partial r}\boldsymbol{\varphi}. \tag{33}$$

With the help of Eqs. (18) and (30), we obtain

$$\boldsymbol{\varphi} = \frac{\ln r}{\pi}\mathbf{p} + \mathbf{L}(\theta)\mathbf{q} + \mathbf{S}^T(\theta)\mathbf{p}. \tag{34}$$

3. An infinite space and a wedge

3.1. An infinite space

Considering that line force **f** and free charge λ act on the center of an infinite space, we have [39]

$$f_l + \int_0^{2\pi} (\mathbf{t}_r)_l r d\theta = 0, \tag{35}$$

or

$$\boldsymbol{\varphi}(2\pi) - \boldsymbol{\varphi}(0) = \hat{\mathbf{f}}, \tag{36}$$

where

$$\hat{\mathbf{f}}^T = [f_1, f_2, f_3, f_4, f_5, -\lambda].$$

At the same time, a dislocation with Burgers vector $\hat{\mathbf{b}}^T = [b_1, b_2, b_3, b_4, b_5, b_6]$ also act on the center of the infinite space, we get

$$\mathbf{u}(2\pi) - \mathbf{u}(0) = \hat{\mathbf{b}}. \tag{37}$$

From Eqs. (28) and (34), we obtain

$$\begin{aligned}\mathbf{u} = &-\frac{\ln r}{\pi}\mathbf{V}^{-1}\left[\hat{\mathbf{f}} - \mathbf{S}^T(2\pi)\mathbf{H}^{-1}(2\pi)\hat{\mathbf{b}}\right] - \boldsymbol{S}(\theta)\mathbf{V}^{-1}\left[\hat{\mathbf{f}} - \mathbf{S}^T(2\pi)\mathbf{H}^{-1}(2\pi)\hat{\mathbf{b}}\right] \\ &+ \mathbf{H}(\theta)\mathbf{U}^{-1}\left[\mathbf{S}(2\pi)\mathbf{L}^{-1}(2\pi)\hat{\mathbf{f}} + \hat{\mathbf{b}}\right],\end{aligned} \tag{38}$$

$$\begin{aligned}\boldsymbol{\varphi} = &\frac{\ln r}{\pi}\mathbf{U}^{-1}\left[\mathbf{S}(2\pi)\mathbf{L}^{-1}(2\pi)\hat{\mathbf{f}} + \hat{\mathbf{b}}\right] + \mathbf{L}(\theta)\mathbf{V}^{-1}\left[\hat{\mathbf{f}} - \mathbf{S}^T(2\pi)\mathbf{H}^{-1}(2\pi)\hat{\mathbf{b}}\right] \\ &+ \mathbf{S}^T(\theta)\mathbf{U}^{-1}\left[\mathbf{S}(2\pi)\mathbf{L}^{-1}(2\pi)\hat{\mathbf{f}} + \hat{\mathbf{b}}\right].\end{aligned} \tag{39}$$

The derivation procedure of the above equations is shown in (A5-A8). It is worth mentioning that if FG exponential factor $\eta = 0$, the material constants are independent of the θ, then we can acquire the solutions of homogeneous space.

3.2. A wedge

Consider a piezoelectric QC wedge of wedge angle $\alpha(0 \le \theta \le \alpha)$, subjected to the line force and charge at the wedge apex $r = 0$ while wedge edges are traction free. From Eq. (18), we know that

$$\mathbf{p} = \mathbf{0}. \tag{40}$$

In Eq. (36), 2 π is replaced by α. Then

$$\boldsymbol{\varphi}(\alpha) - \boldsymbol{\varphi}(0) = \hat{\mathbf{f}}, \tag{41}$$

or Eq. (41) can be obtained from Eq. (34)

$$\mathbf{L}(\alpha)\mathbf{q} = \hat{\mathbf{f}}. \tag{42}$$

Therefore,

$$\mathbf{u} = -\frac{\ln r}{\pi}\mathbf{L}^{-1}(\alpha)\hat{\mathbf{f}} - \boldsymbol{S}(\theta)\mathbf{L}^{-1}(\alpha)\hat{\mathbf{f}}, \tag{43}$$

$$\boldsymbol{\varphi} = \mathbf{L}(\theta)\mathbf{L}^{-1}(\alpha)\hat{\mathbf{f}}. \tag{44}$$

4. Numerical results and analyzation

2D decagonal piezoelectric QC is used in the numerical research. The relevant material constants are shown below in Table 1, [35].

To avoid ill-conditioned matrices, we introduce the following dimensionless values

$$x_1^* = \frac{x_1}{l}, x_3^* = \frac{x_3}{l}, u_m^* = \frac{u_m}{l}, w_i^* = \frac{R_1 w_i}{(C_{11} l)}, \sigma_{mj}^* = \frac{\sigma_{mj}}{C_{11}}, H_{mj}^* = \frac{H_{mj}}{R_1}, D_j^* = \frac{D_j}{e_{33}}, \phi^* = e_{33}\frac{\phi}{(C_{11} l)}, \tag{45}$$

where $l = 1$ m.

Table 1
Material constants of the 2D piezoelectric QC material.

Material constants	
Phonon field (GPa)	$C_{11} = 234.33, C_{12} = 57.41, C_{13} = 66.63,$ $C_{33} = 232.22, C_{44} = 70.19, C_{66} = 88.46,$
Phason field (GPa)	$K_1 = 122,\ K_2 = 24,\ K_3 = 12$
Couple field (GPa)	$R_1 = R_2 = R_1 = 8.85,$
Piezoelectric constant(Cm^{-2})	$e_{31} = -2.2, e_{33} = 9.3, e_{15} = 5.8,$
Dielectric constants ($10^{-9}C^2/(Nm^2)$)	$\xi_{33} = 25.2, \xi_{11} = \xi_{22} = 22.4.$

Table 2
QC wedges and infinite plane under different loadings.

Numerical case	Loading conditions	Description
Case 1	$\hat{\mathbf{f}} = [1, 0, 0, 0, 0, 0]^T$	The numerical results of homogeneous infinite plane (space) which are subjected to line force $\hat{\mathbf{f}} = [1, 0, 0, 0, 0, 0]^T$ at the origin $r = 0$ are compared with the results in Ref. [35].
Case 2	$\hat{\mathbf{f}} = [1, 0, 0, 0, 0, 0]^T$	The numerical results of FG wedges with angle range of $0° \le \alpha \le 360°$ which subjected to line force $\hat{\mathbf{f}} = [1, 0, 0, 0, 0, 0]^T$ at the wedge apex.
Case 3	$\hat{\mathbf{f}} = [0, 0, 0, 0, 0, 1]^T$	The numerical results of FG wedges with angle range of $0° \le \alpha \le 180°$ which subjected to line charge $\hat{\mathbf{f}} = [0, 0, 0, 0, 0, 1]^T$ at the wedge apex.
Case 4	$\hat{\mathbf{f}} = [1, 0, 0, 0, 0, 0]^T$	The effect of FG exponential factor η on mechanical behaviors of infinite space which subjected to line force and line dislocation.
	$\hat{\mathbf{b}} = [1, 0, 0, 0, 0, 0]^T$	

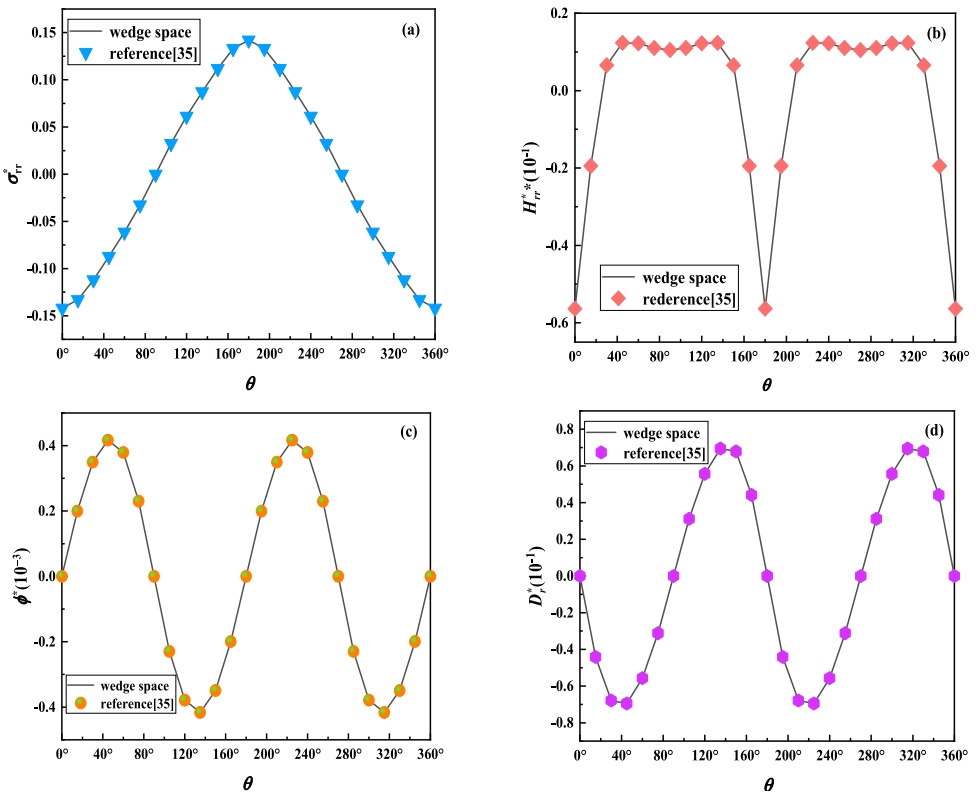

Fig. 3. Comparison of the numerical results in our case with the reference: (a) dimensionless phonon stress σ^*_{rr}, (b) dimensionless phason stress $H^*_{rr}(10^{-1})$, (c) dimensionless electric potential ϕ^* (10^{-3}) and (d) dimensionless electric displacement $D_r{}^*(10^{-1})$.

Next, the numerical examples of 2D decagonal piezoelectric QC wedges and infinite space in different cases are given below in Table 2.

Case 1. In this part, we set polar diameter $r = 2$, $\eta = 0$ which means that material is homogeneous, and discuss the mechanical behavior of homogeneous infinite plane which subjected to line force $\hat{\mathbf{f}} = [1, 0, 0, 0, 0, 0]^T$ at the center $r = 0$. In order to verify the correctness of the program, we compared the numerical results of this case with the Ref. [35], and the relevant results are shown in Fig. 3.

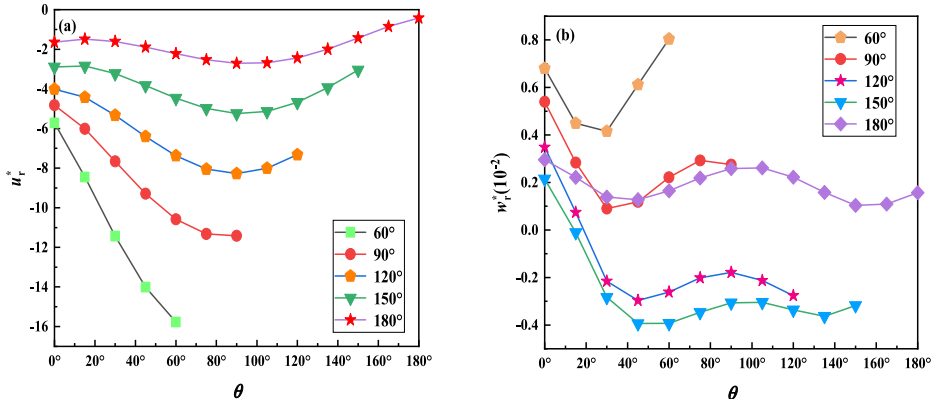

Fig. 4. Changing curves of dimensionless phonon displacement, phason displacement with θ(a) u_r^*, (b) $w_r^*(10^{-2})$.

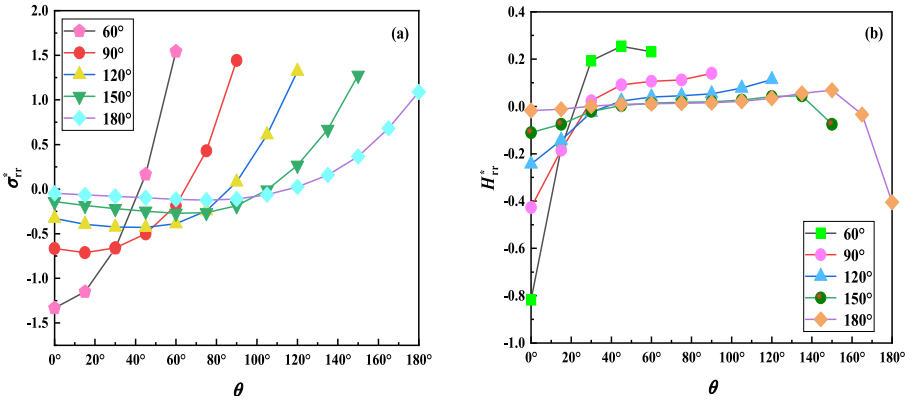

Fig. 5. Changing curves of dimensionless phonon stress and phason stress (a) σ_{rr}^*, (b) H_{rr}^*.

Figure 3 shows the comparisons of dimensionless stresses, dimensionless electric potential and electric displacement for Ref. [35] and Case 1. According to Fig. 3(a) and (b), the changing curves of dimensionless stresses in the infinite plane are consistent with those of the Ref. [35], and they are both symmetric at $\theta = 180^o$. Moreover, the values of σ_{rr}^* are bigger than H_{rr}^*, which indicates that the effect of a single line force on the phonon stress is greater than that on the phason stress. From Fig. 3(c) and (d), the changing curves of dimensionless electric potential and electric displacement are in accordance with the Ref. [35]. $D_r{}^*$ is several orders of magnitude bigger than ϕ^* which indicates that the influence of a single line force on the electric displacement is more evident than that on electric potential. What's more, the change of ϕ^* is similar to that of Sine function in the range $[0, 4\pi]$ and the variation of $D_r{}^*$ is similar to that of Cosine function in the range$[-(3/2)\pi, (5/2)\pi]$.

Case 2. In this part, we set $r = 2$, $\eta = 1$. The wedge subjected to line force $\hat{\mathbf{f}} = [1, 0, 0, 0, 0, 0]^T$ at the wedge apex, and the mechanical behavior of wedge whose angle α=60°, 90°, 120°, 150°, 180° is discussed.

The changing curves of dimensionless displacements with respect to θ are shown in Fig. 4. According to Fig. 4, the absolute values of u_r^* decrease with the increase of wedge angle α, and the values of u_r^* decrease first and then increase with θ when $\alpha = 180°$. The values of w_r^* decrease initially, followed by an increase, but then decrease and then increase with θ when $\alpha = 180°$. Since the phason displacement is much smaller than the phonon displacement, the line force $\hat{\mathbf{f}} = [1, 0, 0, 0, 0, 0]^T$ has little influence on the atomic rearrangement of 2D decagonal piezoelectric QC.

As can be seen from Fig. 5, the changing curves of dimensionless stresses σ_{rr}^* and H_{rr}^* do not show any symmetry because elastic constants depend on θ. From Fig. 5(a), we can find that the absolute values of σ_{rr}^* decrease with the growth of the wedge angle α, and the values of σ_{rr}^* increase with θ. In addition, the values of H_{rr}^* increase gradually and then decrease with θ when $\alpha = 180°$. By comparing Figs. 5, 3(a) and (b), the values of stresses in Fig. 5 are greater than those in Fig. 3(a) and (b), which implies that the line force has more effect on stresses in FG piezoelectric QC wedges than those in homogeneous piezoelectric QC wedges.

Figure 6 shows the changing curves of dimensionless electric potential and electric displacement with θ. The effect of force and electricity coupling is very obvious from Fig. 6. When single line force is applied to a 2D piezoelectric QC wedge, it will generate equal positive and negative charges on the surface of the material. This phenomenon is called the "positive piezoelectric effect". Furthermore, we also notice that the line force has a greater effect on $D_r{}^*$ than that on ϕ^*

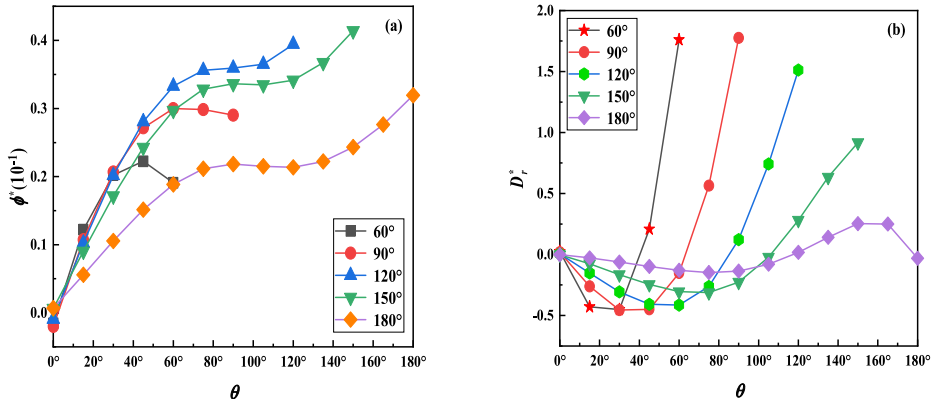

Fig. 6. Changing curves of dimensionless electric potential and *electric* displacement (a) ϕ^* $(10^{-1})$and (b) $D_r{}^*$.

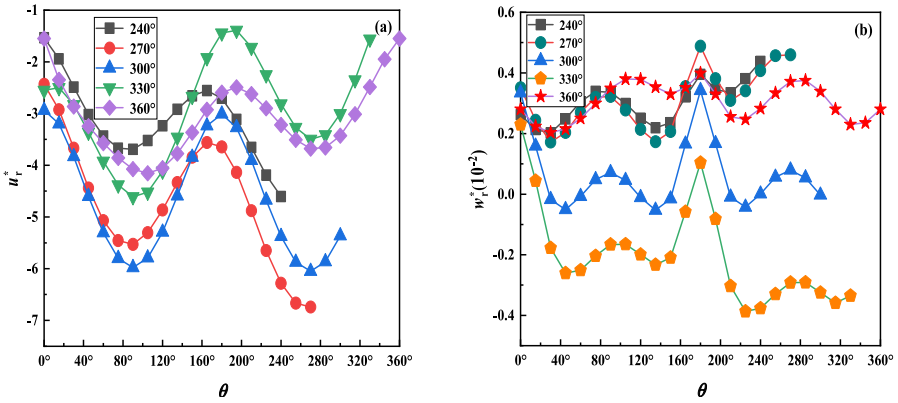

Fig. 7. Changing curves of dimensionless phonon displacement, phason displacement (a) u_r^*, (b) $w_r^*(10^{-2})$.

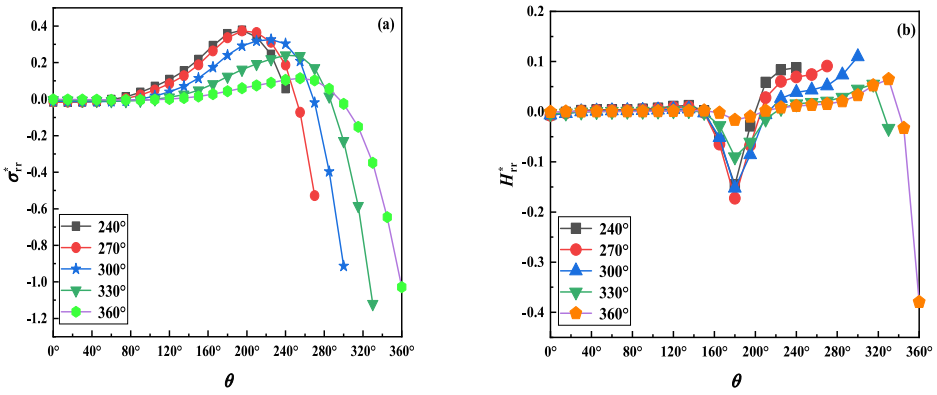

Fig. 8. Changing curves of dimensionless phonon stress and phason stress (a) σ_{rr}^*, (b) H_{rr}^*.

owing to the values of $D_r{}^*$ being bigger. The values of electric potential ϕ^* in Fig. 7(a) are bigger than those in Fig. 3(c), which indicates that the line force may have a more evident influence on electric potential in FG material than that in homogeneous material.

Next, the mechanical behaviors of wedge with different angles $\alpha = 240°, 270°, 300°, 330°, 360°$ are discussed below.

The changing curves of dimensionless displacements are illustrated in Fig. 7. The values of u_r^* decrease first and then increase with θ when $0° \le \theta \le 180°$, and the values of w_r^* decrease initially, followed by an increase, but then decrease and then increase with θ when $0° \le \theta \le 180°$. In addition, w_r^* has a maximum when $\theta = 180°$ for the same wedge angle. We find that the line force has little effect on lattice rearrangement when $180° \le \alpha \le 360°$, which is in accordance with Fig. 4(b).

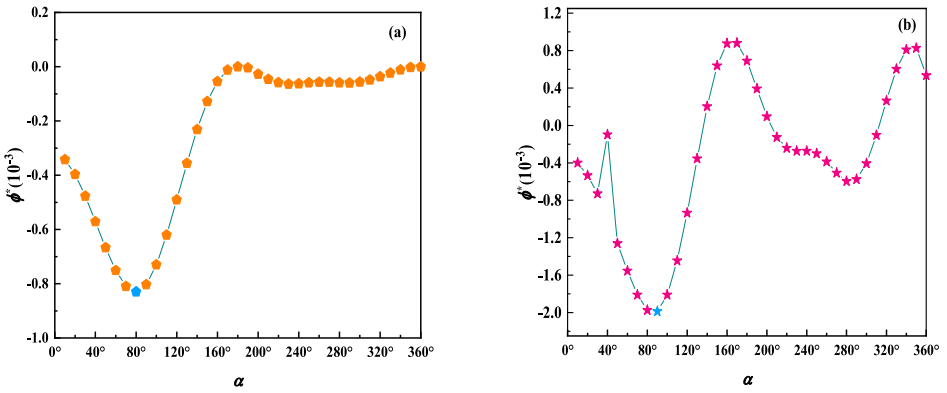

Fig. 9. Changing curves of dimensionless electric potential ϕ^* (10^{-3}) (a) homogeneous material (b) FG material, which located at $r = 2$, $\theta = 0°$.

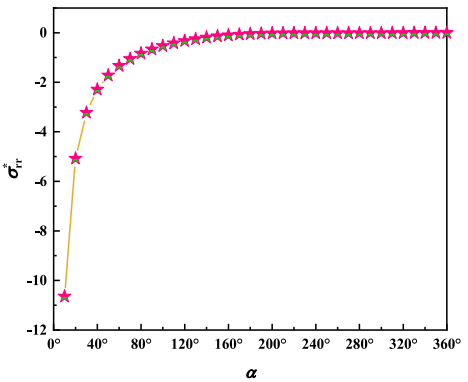

Fig. 10. Changing curves of dimensionless phonon stress σ^*_{rr} which located at $r = 2$, $\theta = 0°$.

The changing curves of dimensionless stresses with θ are shown in Fig. 8. It is obvious that, the variation of phason stress is more sophisticated than that of phonon stress. From Fig. 8(a), the values of σ^*_{rr} first increase and then decrease with θ. From Fig. 8(b), the values of H^*_{rr} become bigger with α when $\theta = 180°$, $\alpha \geq 270°$, and increase initially, followed by a decrease, but then raise and then reduce with θ when $\alpha \geq 330°$. What's more, by comparing Fig. 5 with Fig. 8, the absolute values of σ^*_{rr} are maximum when $\alpha = 60°$, $\theta = 60°$, and the values of σ^*_{rr} and H^*_{rr} go to 0 within $0° \leq \theta \leq 90°$ as wedge angle α increases.

As shown in Fig. 9, a point which located at $r = 2$, $\theta = 0°$ is selected and the changes of ϕ^* for homogeneous material and FG material at this point are investigated. By comparing the variations of Fig. 9(a) and (b), it is obvious that the trend in Fig. 9(b) is more complex than that in Fig. 9(a) due to the inhomogeneity of materials. The absolute values of ϕ^* are the largest when $\alpha = 80°$, $\alpha = 90°$, respectively, for homogeneous material and FG material. In addition, the values of ϕ^* in Fig. 6(a) are several orders of magnitude bigger than those in Fig. 9(b) due to the discontinuous boundary conditions. Therefore, the line force has a more significant effect on electric potential at surface $\theta = \alpha$ than that at $\theta = 0°$. It's worth mentioning that, with the aid of strain gradient theory and first-order shear deformation theory, Arefi and Zenkour [46,47] have investigated the electric potential distribution of piezoelectric materials in detail.

The variation of σ^*_{rr} with wedge angle α at the point $r = 2$, $\theta = 0°$ is shown in Fig. 10. It is worth noting that the absolute values of σ^*_{rr} gradually decrease with the increasing of α, and they are going to zero which start at about 90° from Fig. 10. Through Eq. (41), we know that the bigger $\boldsymbol{\varphi}(\alpha)$, the smaller $\boldsymbol{\varphi}(0)$ is. In our calculation, we find that the values *of* $\boldsymbol{\varphi}(0)$ are small, which means that the values of $\boldsymbol{\varphi}(\alpha)$ are big and line force has little effect on $\theta = 0°$ when α increases. Through the analysis of Figs. 9 and 10, the boundary conditions have a significant effect on electric potential and phonon stress σ^*_{rr}.

Case 3. In this part, when the wedge subjected to line charge $\hat{\mathbf{f}} = [0, 0, 0, 0, 0, 1]^T$, the mechanical behaviors of wedge with different wedge angles $\alpha = 60°, 90°, 120°, 150°, 180°$ are analyzed.

Figure 11 shows the variations of dimensionless stresses with θ. From Fig. 11(a), σ^*_{rr} has the greatest absolute value when α, $\theta = 120°$. From Fig. 11(b), H^*_{rr} has the largest absolute value when α, $\theta = 180°$, and the change of H^*_{rr} firstly reduces and then increases with θ when $\alpha = 180°$. The values of σ^*_{rr} and H^*_{rr} in Fig. 11 are smaller than those in Figs. 5 and 8, which can be explained that a temperature field will be generated when the current flows in the conductor, so the current does not completely act on stress, resulting in small stresses. The mechanical deformation was produced by piezoelectric QC wedge under line charge, which is the inverse piezoelectric effect.

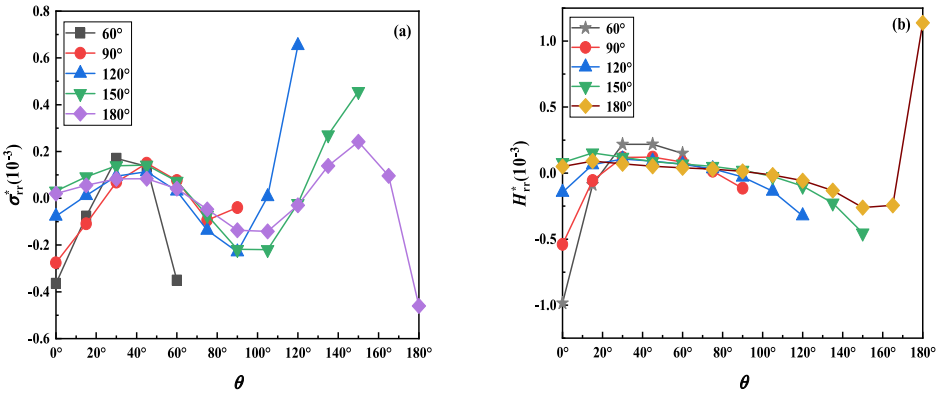

Fig. 11. Changing curves of dimensionless phonon stress and phason stress (a) $\sigma_{rr}^*(10^{-3})$, (b) $H_{rr}^*(10^{-3})$.

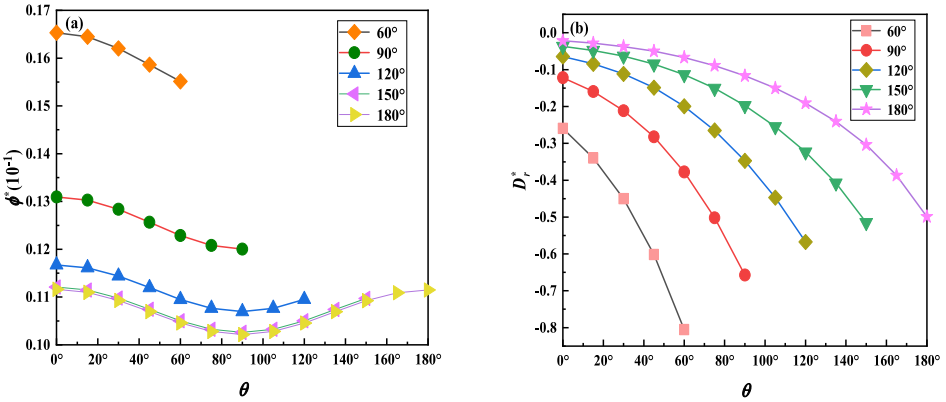

Fig. 12. Changing curves of dimensionless electric potential and electric displacement (a) ϕ^* (10^{-1}) and (b) $D_r{}^*$.

From Fig. 12(a), it is obvious that the values of ϕ^* reduce as wedge angle α increases and they decrease first and then increase with θ. Also, the values of $D_r{}^*$ fall when α descends and they decline gradually with the growth of θ. The values of $D_r{}^*$ are larger than the values of ϕ^*, which implies that line charge has a more evident effect on $D_r{}^*$ than ϕ^*.

Case 4. In this part, the infinite space subjected to line force $\hat{\mathbf{f}} = [1, 0, 0, 0, 0, 0]^T$ and line dislocation $\hat{\mathbf{b}} = [1, 0, 0, 0, 0, 0]^T$, simultaneously. The effect of FG exponential factor η on mechanical behavior of a QC is researched.

As shown in Fig. 13(a) and (b), the values of σ_{rr}^* first increase and then decrease with θ and have maximum absolute value at $\theta = 0°$ when the graded FG factor $\eta < 0$, but they have the greatest absolute values at $\theta = 360°$ when $\eta > 0$. The values of H_{rr}^* have similar trends with θ when $0° \le \theta \le 180°$, and η has little effect on H_{rr}^* when $90° \le \theta \le 270°$. From Fig. 13(c) and (d), the absolute values of ϕ^* enlarge as η increases when $\eta > 0$, but the absolute values of ϕ^* enlarge with the decreasing of η when $\eta < 0$. In addition, the values of ϕ^* reduce first and then increase gradually with θ when $\eta > 0$. The values of $D_r{}^*$ increase with η when $15° \le \theta \le 30°$, the absolute values of $D_r{}^*$ enlarge as η increases when $\eta < 0$, $180° \le \theta \le 360°$. Based on the above analysis, the FG exponential factor has more effect on electric potential and electric displacement than stresses.

5. Conclusions

In summary, the infinite homogeneous 2D decagonal piezoelectric QCs space, infinite FG space and FG wedge which subjected to line force, charge or dislocation are investigated. Real form expressions of stresses and displacements are directly derived without introducing complex vectors. By means of numerical examples and illustrations, the coupling effect of different loads is clearly expressed. The research conclusions are as follows:

(1) σ_{rr}^*, H_{rr}^* and ϕ^* in FG 2D piezoelectric QC wedge are several orders of magnitude bigger than those in 2D piezoelectric QC wedge, so the line force has more effect on σ_{rr}^*, H_{rr}^* and ϕ^* of FG 2D piezoelectric QC wedge.

(2) Wedge angle and boundary conditions have great influences on displacements and stresses. The absolute values of u_r^* caused by line force decrease with the increase of wedge angle α when $0° \le \alpha \le 180°$. σ_{rr}^* can get smaller and smaller at the interface $\theta = 0°$ when α gets bigger and bigger due to discontinues stress boundary condition.

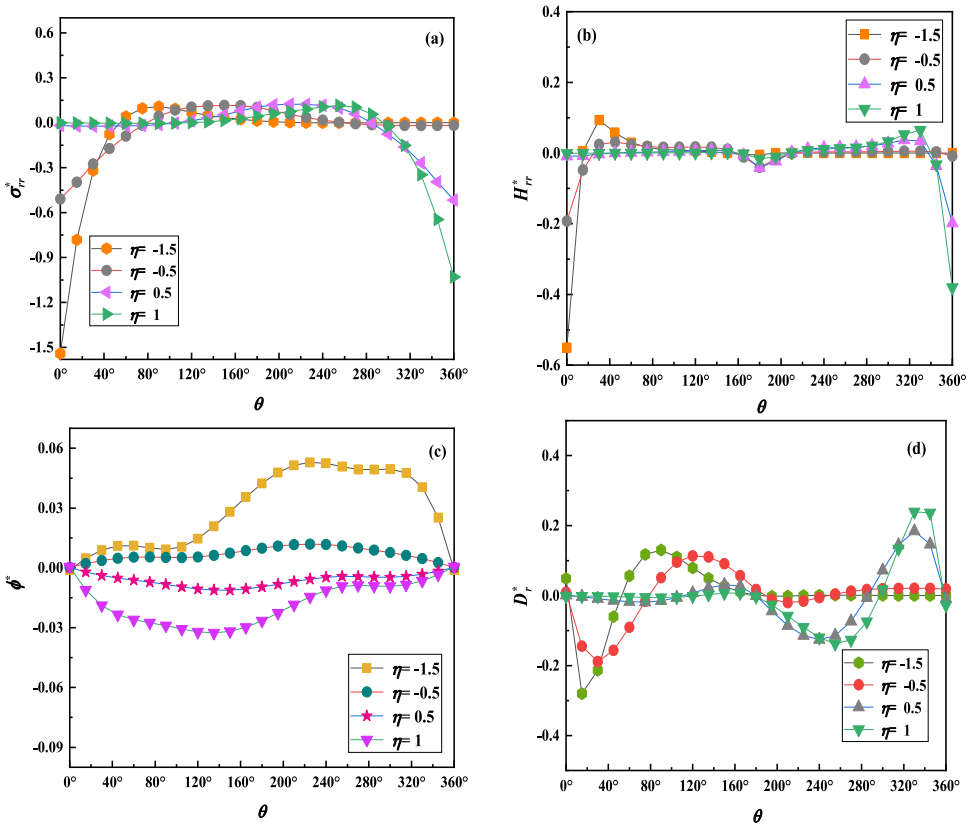

Fig. 13. Changing curves of dimensionless phonon stress, phason stress, electric potential and electric displacement (a) σ_{rr}^*, (b) H_{rr}^*, (c) ϕ^* and (d) D_r^*.

(3) The values of ϕ^* at $\theta = \alpha$ are several orders of magnitude greater than those at $\theta = 0°$, which indicates that the line force has more significant effect on electric potential at surface $\theta = \alpha$ than that at $\theta = 0°$.
(4) The effect of line force on phonon displacement is greater than that on phason displacement, which means that line force has little effect on lattice rearrangement. In addition, the FG exponential factor η has more effect on electric potential and electric displacement than stresses.

Piezoelectric QCs are expected to be used as sensors and actuators of intelligent structures and systems [48]. This study may provide some theoretical guidance and references to design and optimize wedge structures, such as electronic wedge actuators and fiber optic sensors [49]. Furthermore, these new results can help us to further understand the complex properties and the mechanical behaviors of FG 2D piezoelectric QC wedges and spaces.

Acknowledgements

This work was supported by the National Natural Science Foundation of China (Grant Nos. 11972365 and 12102458) and China Agricultural University Education Foundation (No. 1101–2412001).

Appendix

For an FG 2D piezoelectric QC wedge subjected to line force**f**at the wedge apex, according to the requirement of stress equilibrium and $(\mathbf{t}_r)_\alpha = \sigma_{\alpha j} n_j$, $(\mathbf{t}_r)_\gamma = H_{\gamma j} n_j$, we have [39]

$$f_I + \int_0^\alpha (\mathbf{t}_r)_I r d\theta = f_I + \int_0^\alpha \sigma_{Ij} n_j r d\theta = 0, (I = 1, 2, 3, 4, 5, 6), \tag{A1}$$

where $\sigma_{Ij} (I = 1, 2, 3)$ represent stresses in the phonon field, and $\sigma_{Ij} (I = 4, 5, 6)$ denote stresses in the phason field and electric displacement. Therefore, Eqs. (10) and (11) can be derived by dimensional analyzes.

In the above equation,

$$r_{,j} = n_j, \theta_{,j} = \frac{1}{r} m_j, \; m_{j,\theta} = -n_j, n_{j,\theta} = m_j, \tag{A2}$$

where

$$\mathbf{n}^T = [\cos\theta, 0, \sin\theta, 0, 0, 0], \mathbf{m}^T = [-\sin\theta, 0, \cos\theta, 0, 0, 0], \tag{A3}$$

and (**n, m**) are the unit vectors normal and tangent to a circle.

We have [38]

$$\begin{aligned} \boldsymbol{S}(\theta) &= \frac{1}{\pi}\int_0^\theta \mathbf{N}_1(\varpi)d\varpi, \\ \mathbf{H}(\theta) &= \frac{1}{\pi}\int_0^\theta \mathbf{N}_2(\varpi)d\varpi, \\ \mathbf{L}(\theta) &= \frac{1}{\pi}\int_0^\theta \mathbf{N}_3(\varpi)d\varpi. \end{aligned} \tag{A4}$$

Substituting Eqs. (28) and (34) into Eqs. (36) and (37) to yield

$$\mathbf{S}^T(2\pi)\mathbf{p} + \mathbf{L}(2\pi)\mathbf{q} = \hat{\mathbf{f}}, \tag{A5}$$

$$\mathbf{H}(2\pi)\mathbf{p} - \mathbf{S}(2\pi)\mathbf{q} = \hat{\mathbf{b}}. \tag{A6}$$

From Eqs. (A5) and (A6), the undetermined vectors **p, q** are derived as

$$\mathbf{p} = \mathbf{U}^{-1}\left[\mathbf{S}(2\pi)\mathbf{L}^{-1}(2\pi)\hat{\mathbf{f}} + \hat{\mathbf{b}}\right], \tag{A7}$$

$$\mathbf{q} = \mathbf{V}^{-1}\left[\hat{\mathbf{f}} - \mathbf{S}^T(2\pi)\mathbf{H}^{-1}(2\pi)\hat{\mathbf{b}}\right], \tag{A8}$$

where,

$$\mathbf{U} = \mathbf{S}(2\pi)\mathbf{L}^{-1}(2\pi)\mathbf{S}^T(2\pi) + \mathbf{H}(2\pi), \mathbf{V} = \mathbf{L}(2\pi) + \mathbf{S}^T(2\pi)\mathbf{H}^{-1}(2\pi)\mathbf{S}(2\pi).$$

References

[1] D. Levine, P.J. Steinhardt, Quasicrystals: a new class of ordered structures, Phys. Rev. Lett. 53 (26) (1984) 2477–2480.
[2] M.V. Jaric, D.R. Nelson, Introduction to quasicrystals, Phys. Today 43 (3) (1990) 77–79.
[3] S.L. Chang, W.B. Chin, C.M. Zhang, C.J. Jenks, P.A. Thiel, Oxygen adsorption on a single-grain, quasicrystal surface, Surf. Sci. 337 (1–2) (1995) 135–146.
[4] Y. Chen, J. Qiang, C. Dong, Smearing-type wear behavior of $Al_{62}Cu_{25.5}Fe_{12.5}$ quasicrystal abrasive on soft metals, Intermetallics 68 (2016) 23–30.
[5] R. Wittmann, K. Urban, M. Schandl, E. Hornbogen, Mechanical properties of single-quasicrystalline AlCuCoSi, J. Mater. Res. 6 (06) (1991) 1165–1168.
[6] J.M. Dubois, P. Brunet, W. Costin, A. Merstallinger, Friction and fretting on quasicrystals under vacuum, J. Non Cryst. Solids 334 (2004) 475–480.
[7] E. Macia, Optimizing the thermoelectric efficiency of icosahedral quasicrystal and related complex alloys, Phys. Rev. B. 85 (20) (2009) 1–7.
[8] W.G. Yang, D.H. Ding, R.H. Wang, C.Z. Hu, Thermodynamics of equilibrium properties of quasicrystals, Z. Phys. B Condens. Matter 100 (3) (1997) 447–454.
[9] O. Biham, D. Mukamel, S. Shtrikman, Symmetry and stability of icosahedral and other quasicrystalline phases, Phys. Rev. Lett. 56 (5) (1986) 2191–2194.
[10] T.Y. Fan, A study on the specific heat of a one-dimensional hexagonal quasicrystal, J. Phys. Condens. Matter 11 (45) (1999) L513–L517.
[11] C.L. Li, Y.Y. Liu, Phason-strain influence on low-temperature specific heat of the decagonal Al-Ni-Co quasicrystal, Chin. Phys. Lett. 18 (4) (2001) 570–573.
[12] S. Ueda, A cracked functionally graded piezoelectric material strip under transient thermal loading, Acta Mech. 199 (1–4) (2008) 53–70.
[13] R.M. Mcmeeking, The energy release rate for a Griffith crack in a piezoelectric material, Eng. Fract. Mech. 71 (7–8) (2004) 1149–1163.
[14] J.K. Du, X.Y. Jin, J. Wang, K. Xian, Love wave propagation in functionally graded piezoelectric material layer, Ultrasonics 46 (1) (2007) 13–22.
[15] B.G. Nam, K. Watanabe, Effect of electric boundary conditions on crack energy density and its derivatives for piezoelectric material, Eng. Fract. Mech. 75 (2) (2008) 207–222.
[16] E. Mohammad-Rezaei. Bidgoli, M. Arefi, Free vibration analysis of micro plate reinforced with functionally graded graphene nanoplatelets based on modified strain-gradient formulation, J. Sandw. Struct. Mater. 23 (2) (2021) 436–472.
[17] E. Pan, F. Han, Green's functions for transversely isotropic piezoelectric multilayered half-spaces, J. Eng. Math. 42 (11–12) (2004) 3207–3233.
[18] C.D. Chen, On the singularities of the thermo-electro-elastic fields near the apex of a piezoelectric bonded wedge, Int. J. Solids Struct. 43 (5) (2006) 957–981.
[19] M. Arefi, R. Karroubi, M. Irani-Rahaghi, Free vibration analysis of functionally graded laminated sandwich cylindrical shells integrated with piezoelectric layer, Appl. Math. Mech. 37 (7) (2016) 821–834.
[20] M.J. Zhou, S.J. Duan, Y.P. Kong, S.H. Liu, Stress distribution in a piezoelectric material with an elliptical hole subjected to remote uniform shear mechanical and electric loads, Adv. Mat. Res. 97–101 (2010) 956–959.
[21] X.F. Li, L.Y. Xie, T.Y. Fan, Elasticity and dislocations in quasicrystals with 18-fold symmetry, Phys. Lett. A 377 (2013) 2810–2814.
[22] X. Wang, E. Pan, Analytical solutions for some defect problems in 1D hexagonal and 2D octagonal quasicrystals, Pramana 70 (5) (2008) 911–933.
[23] X.Y. Li, T. Wang, R.F. Zheng, G.Z. Kang, Fundamental thermo-electro-elastic solutions for 1D hexagonal QC, ZAMM. J. Appl. Math. Mech. Z. Angew. Math. Mech. 95 (5) (2015) 457–468.
[24] L.L. Zhang, L.Z. Yang, L.Y. Yu, Y. Gao, General solutions of thermoelastic plane problems of two-dimensional quasicrystals, J. Nanjing Univ. Aeronaut. Astronaut. 031 (002) (2014) 132–136.
[25] Y. Li, L.Z. Yang, Y. Gao, Thermo-elastic analysis of functionally graded multilayered two-dimensional decagonal quasicrystal plates, ZAMM. J. Appl. Math. Mech. Z. Angew. Math. Mech. 98 (9) (2018) 1–18.
[26] J. Yu, J.H. Guo, E. Pan, Y.M. Xing, General solutions of plane problem in one-dimensional quasicrystal piezoelectric materials and its application on fracture mechanics, Appl. Math. Mech. 36 (6) (2015) 793–814.
[27] Y. Li, M.H. Zhao, Q.H. Qin, C.Y. Fan, Analysis solution method for 3D planar crack problems of two-dimensional hexagonal quasicrystals with thermal effects, Appl. Math. Model. 69 (5) (2019) 648–664.
[28] K.Q. Hu, S.A. Meguid, Z. Zhong, C.F. Gao, Partially debonded circular inclusion in one-dimensional quasicrystal material with piezoelectric effect, Int. J. Mech. Mater. Des. 20 (2020) 749–766.

[29] X.L. Xu, R. Rajapakse, On singularities in composite piezoelectric wedges and junctions, Int. J. Solids Struct. 37 (23) (2000) 3253–3275.
[30] X. Lv, G.T. Liu, Exact solutions for interaction of parallel screw dislocations with a wedge crack in one-dimensional hexagonal quasicrystal with piezoelectric effects, Math. Probl. Eng. 5 (2020) 1–15.
[31] M.C. Chen, J.J. Zhu, K.Y. Sze, Electroelastic singularities in piezoelectric–elastic wedges and junctions, Eng. Fract. Mech. 73 (7) (2006) 855–868.
[32] C. Hwu, T. Ikeda, Electromechanical fracture analysis for corners and cracks in piezoelectric materials, Int. J. Solids Struct. 45 (22–23) (2008) 5744–5764.
[33] C. Hwu, T.C.T. Ting, Solutions for the anisotropic elastic wedge at critical wedge angles, J. Elast. 24 (1–3) (1990) 1–20.
[34] T.C.T. Ting, The critical angle of the anisotropic elastic wedge subject to uniform tractions, J. Elast. 20 (2) (1988) 113–130.
[35] W.S. Xu, D. Wu, Y. Gao, Fundamental elastic field in an infinite plane of two-dimensional piezoelectric quasicrystal subjected to multi-physics loads, Appl. Math. Model. 52 (12) (2017) 186–196.
[36] L.L. Zhang, D. Wu, W.S. Xu, L.Z. Yang, A. Ricoeur, Green's functions of one-dimensional quasicrystal bi-material with piezoelectric effect, Phys. Lett. A 380 (39) (2016) 3222–3228.
[37] Y. Li, L.Z. Yang, L.L. Zhang, Gao Y, Nonlocal free and forced vibration of multilayered two-dimensional quasicrystal nanoplates, Mech. Adv. Mater. Struct. 28 (12) (2021) 1216–1226.
[38] T.C.T. Ting, in: Anisotropic Elasticity: Theory and Applications, Oxford University, Press on Demand, 1996, p. 235.
[39] M.Y. Chung, T.C.T. Ting, Line force, charge and dislocation in angularly inhomogeneous anisotropic piezoelectric wedges and spaces, Philos. Mag. A 71 (6) (1995) 1335–1343.
[40] T.C.T. Ting, Line forces and dislocations in angularly inhomogeneous anisotropic elastic wedges and spaces, Q. Appl. Math. 47 (1) (1989) 123–128.
[41] G. Altay, M.C. Dokmeci, On the fundamental equations of piezoelasticity of quasicrystal media, Int. J. Solids Struct. 49 (23–24) (2012) 3255–3262.
[42] C.Z. Hu, R.H. Wang, D.H. Ding, Symmetry groups, physical property tensors, elasticity and dislocations in quasicrystals, Rep. Prog. Phys. 63 (1) (2000) 1–39.
[43] T.Y. Fan, Mathematical theory and methods of mechanics of quasicrystalline materials, Engineering 5 (4) (2013) 407–448.
[44] P.H. Lee, M. Odlin, H. Yin, Development of a hollow cylinder test for the elastic modulus distribution and the ultimate strength of bamboo, Constr. Build. Mater. 51 (1) (2014) 235–243.
[45] M.L. Williams, Stress singularities resulting from various boundary conditions in angular corners of plates in extension, J. Appl. Mech. 19 (4) (1952) 526–528.
[46] M. Arefi, A.M. Zenkour, Size-dependent electro-elastic analysis of a sandwich microbeam based on higher-order sinusoidal shear deformation theory and strain gradient theory, J. Intell. Mater. Syst. Struct. 29 (7) (2018) 1394–1406.
[47] M. Arefi, Two-dimensional bending behavior of the three-layered shear deformable nanoshells: electro-elastic size-dependent, J. Sandw. Struct. Mater. 23 (7) (2021) 2882–2900.
[48] J.H. Guo, Z.Y. Zhang, Y.M. Xing, Antiplane analysis for an elliptical inclusion in 1D hexagonal piezoelectric quasicrystal composites, Philos. Mag. 96 (2016) 349–369.
[49] Y. Wei, Y.D. Su, C.L. Liu, L. Liu, Z.D. Zhu, Y.H. Zhang, Micro-displacement optical fiber sensor based on surface plasmon resonance, Laser Optoelectron. Prog. 55 (4) (2018) 85–91.